Final Draft

of the original manuscript

Chen, Y.; Lu, X.; Lamaka, S.; Ju, P.; Blawert, C.; Zhang, T.; Wang, F.; Zheludkevich, M.:

Active protection of Mg alloy by composite PEO coating loaded with corrosion inhibitors.

In: Applied Surface Science. Vol. 504 (2020) 144462.

First published online by Elsevier: 28.10.2019

https://dx.doi.org/10.1016/j.apsusc.2019.144462

Active protection of Mg alloy by composite PEO coating loaded with corrosion inhibitors

Yan Chen[1,2,3], Xiaopeng Lu[1], Sviatlana V. Lamaka[2], Pengfei Ju[3], Carsten Blawert[2], Tao Zhang[1], Fuhui Wang[1], Mikhail L. Zheludkevich[2,4]

[1]*Shenyang National Laboratory for Materials Science, Northeastern University, 3-11 Wenhua Road, Shenyang 110819, China*

[2]*MagIC – Magnesium Innovation Centre, Institute of Materials Research, Helmholtz-Zentrum Geesthacht, Max-Planck-Str. 1, 21502 Geesthacht, Germany*

[3]*Shanghai Aerospace Equipment Manufacturer, Shanghai, 200245, China*

[4]*Faculty of Engineering, University of Kiel, Kaiserstrasse 2, 24143 Kiel, Germany*

Abstract

A PEO (Plasma Electrolytic Oxidation) /Sol-gel composite coating was prepared on AZ91 magnesium alloy. The porous layer produced by PEO was loaded with corrosion inhibitors (sodium salts of glycolic, 4-aminosalicylic and 2,6-pyridinedicarboxylic acids). Sealed with a thin sol-gel layer, this sandwich-like structure demonstrated durable barrier and active corrosion protection as shown by electrochemical impedance spectroscopy (EIS) and scanning vibrating electrode technique (SVET). The active protection mechanism ensures self-healing ability of the coating system, which was obtained by suppression of the re-deposition of impurity and/or adsorption of the impregnated inhibitors upon the exposed surface.

Keywords: Magnesium; Plasma electrolytic oxidation; Sol-gel coating; Corrosion inhibitors; Active corrosion protection

1. Introduction

Plasma electrolytic oxidation (PEO) is an efficient surface treatment process for light metals and their alloys (Al, Mg and Ti) by forming ceramic-like coatings to protect the substrate against corrosion [1-6]. PEO coatings are normally produced from non-toxic alkaline-based solutions under high voltage accompanied by numerous short-lived discharges [7-9]. Relatively high porosity is the main concern for PEO coated Mg alloy to maintain long-term

corrosion capability in aggressive environment [10-13]. Most reported work focus on exploring and/or optimizing the electrolyte composition and/or electrical parameters during the treatment to enhance the corrosion performance of the coatings [14-18]. For example, researchers have added particles into PEO electrolyte, aiming at achieving diverse chemical compositions and enhanced corrosion performance of the coatings [19-22]. Sealing the porous layer by post-treatment can largely improve the corrosion property of PEO-coated Mg alloy [23-28]. Addition of inorganic salts [24, 25, 27] and organic acids [26, 27] to post-treatment baths were found to be responsible for deposition of reaction products and thus sealing the open pores of the coating. Fabrication of a top sol-gel film on PEO coating was also proven to be an effective post-treatment process to enhance the corrosion protection for Mg [25, 29, 30].

Corrosion inhibitors are found to be significantly effective to protect Mg surface and the high porosity of the PEO coating can be considered as natural high capacity container to store the inhibitors [31-45]. Halloysite particles were introduced and impregnated with benzotriazole (corrosion inhibitor for Mg) by Sun et al. [47] to enhance the corrosion resistance and to provide self-healing ability for PEO coated Mg. However, such coating has limited self-healing capabilities due to the low amount of incorporated inhibitors. Direct loading of corrosion inhibitors, namely 8-hydroxyquinoline and Ce^{3+} species into the pores produced by PEO process has been first proposed by Lamaka et al. [29]. It was found that Ce^{3+} containing $MgO/Mg(OH)_2$ layer sealed with thin sol-gel coating resisted corrosion attack and showed self-healing property. Similar concept, loading corrosion inhibitors into the PEO coating has been further verified by Ivanou et al. [27, 30], Mohedano [23], Gnedenkov et al. [48, 49], and more recently by Yang et al. [50].

In the present study, three newly discovered corrosion inhibitors in our work [51] have been selected to impregnate into the PEO coating. The inhibiting efficiency (η) of each inhibitor is based on the results of hydrogen evolution tests and defined by the following equation:

$$\eta = \frac{V_{H_2}^0 - V_{H_2}^{inh}}{V_{H_2}^0} \times 100\%$$

where $V_{H_2}^0$ and $V_{H_2}^{inh}$ are the amounts of H_2 (ml) evolved at 20 h of immersion in pure

NaCl solution and in NaCl solution containing corrosion inhibitor. The inhibiting efficiency of the three chosen inhibitors in their 0.05 M/0.03 M concentration solution is all higher than 50% for AZ91 Mg alloy.

Afterwards, a hybrid coating has been produced by formation of a sol-gel layer to seal and immobilize the inhibitors in the micropores in the PEO coating. Electrochemical impedance spectroscopy and scanning vibrating electrode technique (SVET) have been used to evaluate the anti-corrosion performance and degradation process of the composite coatings.

2 Experimental

2.1 Materials

AZ91 magnesium alloy in size of 15mm×15mm ×4mm were prepared from the cast ingot in this investigation. The chemical composition of the alloy is 8.34 wt.% Al, 0.56 wt.% Zn, 0.236 wt.% Mn, max 0.1 wt.% Si, max 0.005 wt.% Cu, and Mg balance, which was measured using an Arc Spark OES (Spectro Ametek, Germany). The specimens were ground with different grit emery sheets (from 400, 800 up to 1200 grit), rinsed with ethanol before drying under cool air at room temperature.

All the reagents used in this study were of analytic purity, where (3-glycidoxypropyl)-trimethoxysilane is composed of more than 98% pure chemical (CAS number: 2530-83-8). All the solutions used in this work were prepared from deionized water.

2.2 Synthesis of composite coating

2.2.1 PEO treatment

The PEO treatment was performed in an alkaline phosphate-containing electrolyte (20 g/l sodium phosphate and 10 g/l potassium hydroxide) by applying a standard DC power supply (ELEKTRO AUTOMATIK, Germany) with a self-designed pulsing unit. The pulse-on and pulse-off ratio (t_{on}:t_{off}) was set at 1:9 with a frequency of 250 Hz. The AZ91 Mg specimen was drilled with a hole and connected to the anode. A hollow stainless steel tube with circulating cooling water inside (HAAKE, K20) was used as the cathode. The temperature of the electrolyte was maintained at 20 ± 2 °C. PEO-coated specimens were produced under

a constant current density (40 mA/cm^2) regime for 60s and then washed with deionized water prior to air-drying.

The PEO coated specimen was put in an airtight container which is connected to a vacuum unit to evacuate the air from the micropores. Afterwards, the coating was impregnated with inhibitors by immersion in 0.05M aqueous solutions of sodium salts of either glycolic, 4-aminosalicylic or 2,6-pyridinedicarboxylic acids for 60s and then dried in an oven at 40 °C for 120 min. Important, that all the inhibitor-containing solutions were adjusted using NaOH solution to neutralized pH values (approximately 6.5-7.5). These three substances have been previously reported to be effective corrosion inhibitors for AZ91 alloy [51].

2.2.2 Synthesis of sol-gel coating and inhibitor loading

The organic-inorganic films were synthesized by mixing two different sols using controllable hydrolysis of (3-glycidoxypropyl)-trimethoxysilane (GPTMS) and titanium (IV) propoxide (TPOT). The detailed sol-gel preparation procedure was the same as in previous work [29]. PEO-coated AZ91 specimens were immersed in the hybrid sol-gel solution for 60s at a constant dipping rate of 3 mm/s before curing at 120 °C for 80 min.

Several kinds of coated specimens were produced by PEO and sol-gel process: (1) the blank sample, sol-gel sealed PEO coating, AZ_PEO_SG; (2) PEO treated AZ91 immersed in solution of sodium glycolate and sealed with the sol-gel top coating, AZ_PEO_Gly_SG; (3) PEO coating immersed in solution of sodium 4-aminosalicylate and sealed with the sol-gel, AZ_PEO_4AmSal_SG; and (4) PEO coating immersed in solution of sodium 2,6-pyridinedicarboxylate and coated with the sol-gel, AZ_PEO_PDC_SG. The same sol-gel formulation was adopted for all tested samples in this work.

2.3 Techniques

Hydrogen evolution test was evaluated using eudiometers. 0.50 g of chips AZ91 Mg alloy with a surface area of 430 cm^2/g were placed in the eudiometer electrolyte (500 ml) . The used solution was 0.5 wt.% sodium chloride with and without addition of inhibitor. Among the inhibitor-containing solutions, 0.05 M solution of sodium salts of glycolic and 4-aminosalicylic acids in NaCl were used. Sodium salt of 2,6-pyridinedicarboxylic acid was

tested at lower concentrations of 0.03 M due to its limited solubility. The immersion time was between 22 h and 28 h and the electrolyte was continuously stirred during the whole test at the speed of 350 ± 100 rpm.

The microstructure (plan and cross-sectional view) of the PEO and composite coatings was examined by SEM (TESCAN Vega3 SB) after sputtering gold to eliminate charging phenomenon caused by insulating surface. Elemental analysis on the cross-section of the coating was performed using an energy dispersive X-ray (EDX) system from eumeX (IXRFsystems).

Electrochemical impedance spectroscopy (EIS) tests were performed to characterize the corrosion properties of the composite coatings during 2 weeks of immersion in aqueous, pH neutral (pH 5.5-6.0), 0.5 wt% NaCl solution. EIS measurements were recorded using a Gamry interface 1000 potentiostat controlled by a computer with AC amplitude of 10mV sinusoidal perturbations over the open circuit potential and a frequency sweep from 100 kHz to 10 mHz. 9 impedance data points were recorded for each frequency decade during the EIS test. A conventional corrosion cell with a three-electrode setup was used, consisted of a platinum mesh as the counter electrode, a saturated Ag/AgCl reference electrode and coated specimen itself with a 0.5 cm^2 exposed area as the working electrode. All tests were carried out in a Faraday cage to eliminate any deviation caused by electromagnetic effect. The EIS data were fitted using Zimpwin software, version 3.10.

Commercial equipment from Applicable Electronics was used to perform the Scanning Vibrating Electrode Technique (SVET) measurements. To evaluate the active corrosion protection and inhibitor performance of the sandwich-like protective coating enriched with three inhibitors, two artificial defects were intentionally made on the surface of the specimens prior to SVET tests. The defects were of 200 µm diameter, 50 µm deep and 1 mm apart. The defects were intentionally drilled by a diamond tool controlled with an optical microscope until reaching the Mg substrate. One map per hour was recorded during samples exposure to neutral 0.05 M sodium chloride solution. In order to keep the concentration of the electrolyte relatively constant, a vessel containing 150 ml 0.05 M NaCl solution was connected to the 10 ml SVET cell. The scanned area, insulated from the rest of the sample

by beeswax was about 3 mm × 3 mm. The vibrating electrode used for SVET measurement was a Pt/Ir probe (Microprobe Inc., USA) with a spherical tip of Pt black of approximately 15 μm diameter. The probe tip was placed 100 ± 5 μm above the surface and vibrated in two orthogonal directions (normal and parallel to the sample surface) with an amplitude of 13 μm. The vibration frequency of the probe was 100 Hz (Z) and 130 Hz (X). The local currents were visualized using a 51 × 51 grid, concluding 2601 current values. Each scan lasted for 30 minutes.

3. Results and discussion

3.1 Microstructure of PEO and PEO-SG coating

The surface morphology of the blank PEO coating and the coating sealed with the sol-gel layer is presented in Fig. 1. Multiple uniformly distributed pores dominate the surface of the PEO coating. The higher magnification image (Fig. 1b) provides more information on the pore morphology of the coating surface. Most of the pores are in the range of 0.5-2 μm. This justifies relatively low intensity of the discharges at the beginning of the treatment. Fig. 1c shows the surface topography of the sol-gel sealed PEO coating. The surface of the composite coating is homogeneous and free of visible defects or blister zones. This means that the sol-gel coating fully covered the PEO layer, no protruding fragments of PEO remained uncovered. The separate-white spots are most likely to be the dust particles.

Fig. 2 displays the microstructure and EDS mapping of the cross section of the composite coating. A stratified structure is visible: the porous PEO coating interpenetrated with the sol-gel coating constituting the top compact sol-gel layer. The thickness of this composite coating is around 5 μm, with the top sol-gel layer and bottom PEO coating being almost equally thick. The EDS mapping verifies that PEO coating is enriched with phosphorus and oxygen from the phosphate-based electrolyte and magnesium originated from the substrate. The organic-inorganic sol-gel film is mainly composed of silicon, oxygen and titanium. Penetration of the sol-gel through the porous PEO coating indicated the good fluidity of the sol solution and affinity of the oxide layer to the silicon-based sol. This microstructural characteristic contributes to excellent adhesion between the sol-gel film and the PEO coating.

3.2 Corrosion performance of the composite coating

Hydrogen evolution tests were performed to evaluate the inhibition effect of the three chosen novel inhibitors. Assuming that water reduction is the only cathodic process during Mg dissolution, 1 mol (with a volume of 22.4 L at standard condition) of generated H_2 indicates dissolution of 1 mol of Mg. Although we have showed recently that oxygen is actually being consumed at the surface of corroding magnesium [52], oxygen contribution is minimal during the measurements in the closed space of the eudiometer. Hydrogen evolution curves can be directly correlated with inhibition efficiency of the inhibitors. The immersion solution is 0.5% NaCl solution with or without corrosion inhibitors and the normalized hydrogen evolution rate (HER) of the samples are presented in Fig.3. The sample exposed to pure NaCl solution generated a large quantity of hydrogen rapidly, demonstrating the substrate was seriously deteriorated by the corrosive ions. When immersed in inhibitor-containing NaCl electrolyte, during the first 1-2 h, no significant inhibiting effect can be seen. As time lapses (after 4-5 h), strong suppression of hydrogen formation occurred in the presence of inhibitors, possibly resulting from adsorption/chelating mechanisms [51]. The inhibiting efficiency of glycolate, 4-aminosalicylate and 2,6-pyridinedicarboxylate was 52, 56 and 72% correspondingly, as calculated from the presented hydrogen evolution curves at 20h of immersion.

Corrosion resistance and degradation process of the composite coatings were evaluated using EIS technique. Fig. 4 shows the evolution of Bode plots of the coatings during 2 weeks of immersion time in 0.5 wt. % NaCl electrolyte. It is apparent that the corrosion resistance of the coatings enriched with the inhibitor is relatively stable and much higher than that of the blank coating without any inhibitor addition. |Z| curve demonstrated that the resistance of AZ_PEO_SG decreased by up to 4 orders of magnitude after 14 days (Fig. 4a). In contrast, the corrosion resistance of the AZ_PEO_Gly_SG was slightly reduced after 2 weeks of immersion test (Fig. 4b). Similar degradation process is observed for other inhibitor containing composite coatings.

Some indicators of the corrosion mechanisms of the coatings can be obtained from the evolution of the impedance spectra. In the initial stage of the EIS tests (2 h), all the bode spectra showed three time constants for the coatings enriched with inhibitor. It is obvious to separate the resistance R_{SG} and capacitance C_{SG} of the top sol-gel layer from the signal of

the interpenetrated sol-gel/outer PEO layer R_{MIX} and C_{MIX} as well as the signal of the inner dense PEO coating R_{dense} and C_{dense}. The result well corroborated the previous microstructural and elemental analysis (Fig. 2), where a distinguished stratified layers are demonstrated: a compact top sol-gel coating, a mixed coating composed of the sol-gel film penetrating inside the micropores of the outer oxide coating and a dense inner film. The AZ_PEO_SG reference coating showed fast degradation with the increase of immersion time (4 h) in NaCl solution and opens up rapid paths for corrosive species to penetrate through the composite coating. Consequently, an alternative third time constant from the response of R_p and C_{dl} replaced R_{dense} and C_{dense} in the frequency range of 10^{-2}~10^{0} Hz in the EIS spectrum for AZ_PEO_SG after 4 h test. This can be attributed to the breakdown of the inner dense layer and initiation of the corrosion, which results in appearance of the double-layer capacitance at the metal/electrolyte interface, C_{dl}, and the corresponding polarization resistance, R_p. However, for three other inhibitor-doped coatings, three time constants (corresponding to the sol-gel, mixed and PEO layers) can be observed in the EIS spectra through the overall 2-week immersion. This demonstrates that the coatings impregnated with inhibitors provide better corrosion protection against corrosive ions than the reference composite coating. The impedance spectra were fitted to get quantitative information of the corrosion resistance and to understand the degradation behavior of the composite coatings. Fig. 5 shows the schematic representation and physical interpretation of the equivalent circuits are shown in Fig. 5. R_{sol} represents the resistance of the NaCl solution, while R_{SG}, R_{MIX}, R_{dense} and R_p are the corrosion resistance of the sol-gel layer, the mixed PEO-SG layer, the dense oxide layer and the double-layer at the metal/electrolyte interface, respectively. In order to adjust the phase shift, constant phase elements were adopted to fit the EIS curves. At early stages of corrosion test (2 h), all the composite coatings could be fitted accurately using a model shown in Fig. 5a. From 4 h and after, an alternative equivalent circuit with a time constant related to corrosion at the metal/electrolyte interface (Fig. 5b) is applied to better fit the spectra of AZ_PEO_SG coating. However, for other coatings enriched with the inhibitors, the model in Fig. 5a can be adopted for fitting the EIS data during the entire immersion treatment.

Fig. 6 shows the various resistance values of the composite coatings versus immersion time based on the fitting results of the experimental spectra. It can be seen that coatings doped with sodium 4-aminosalicylate and sodium 2,6-pyridinedicarboxylate displayed higher corrosion resistance than that of the coating with addition of glycolate salt as well as the blank coating at the beginning of the immersion (Fig. 6a). Afterwards, all the coatings showed similar trend in the evolution of the R_{SG}. R_{SG} value drastically dropped in the beginning few hours, which might be caused by penetration of water and aggressive Cl^- through the defects of the composite layer. The anti-corrosion capability of the sol-gel layer with incorporated corrosion inhibitors became stable after long-term immersion, while the blank composite coating was unstable and decreased continually in the entire immersion experiment.

Fig. 6(b) presents the evolution of the corrosion resistance of the intermediate layer (R_{MIX}). All the coatings showed a rapid degradation after immersion into the NaCl solution. This is typical behavior of thin sol-gel coatings [29, 33]. With the increase of immersion time, the inhibitor containing coatings remained stable over 1 week and then decreased slightly. This behavior might be related to the formation of additional magnesium hydroxide from the hydrolysis of pre-existed magnesium oxide. Hydroxide can seal and densify cracks and micropores in the PEO layer. Note that the R_{MIX} value dropped significantly after 3 days of immersion for the reference system. Since the inner dense oxide layer is the final barrier against corrosion in the coating system, R_{dense} value is directly related with protective ability of the composite coating (Fig. 6c). The dense layer resistance of the inhibitor-doped coatings remained stable between 10 and 100 MΩ cm^2 after 2-week immersion test, indicating that addition of corrosion inhibitors provides active corrosion protection for PEO coated Mg. It should be mentioned that R_p value for reference coating after 2 h are shown in Fig. 6c for comparison. The results demonstrate that all three sandwich-like coatings enriched with corrosion inhibitors yield significantly better protection effect compared to the reference coating with no inhibitor.

The degradation behavior of the composite coatings was studied by localized electrochemical technique (SVET) to reveal the active component of corrosion protection (in contrast to barrier properties characterized by EIS) provided by the corrosion inhibitors.

Fig. 7 demonstrates the change of localized current density values along with immersion time, which was recorded by scanning the 3mm × 3mm area with two defects. The first SVET measurement was taken immediately after immersion of the sample into 0.05M NaCl solution. For AZ_PEO_4AmSal_SG and AZ_PEO_PDC_SG samples, moderate anodic and cathodic current density values combined with gas evolution was observed in the artificial defects, indicating that corrosion occurs at the exposed Mg substrate. This might result from the presence of cathodic phases ($Mg_{17}Al_{12}$ or Al-Mn phase) in the defects. Besides, as shown in Fig.3, most of the inhibitors demonstrate strong inhibiting effect after initial "induction periods", several hours after beginning of exposure. The corrosion activity of inhibitor-containing samples was suppressed to much lower values by 24 and 48 h of immersion. For AZ_PEO_Gly_SG sample, even weaker corrosion activity was recorded at the beginning of immersion that slightly increased throughout 48 hours of immersion. However, even at the end of the second day (48h), the activity of AZ_PEO_Gly_SG sample remained 20 times lower than that for the blank sample AZ_PEO_SG. The corrosion activity on the sample without inhibitors gradually increased from 4 to 5 $\mu A/cm^2$ (at 0 and 1h) to above 400 $\mu A/cm^2$ (by 48h) as a sum of positive and negative current density.

Optical images of the PEO-SG coatings taken at the beginning of immersion and after 48h-immersion are also shown in Fig.7. Obvious bubbles could be observed above the artificial defects after 48 h for the AZ_PEO_SG sample, which were most likely to be hydrogen bubbles due to the corrosion of Mg substrate. Black corrosion products were piled and spread to adjacent regions of the defects. Nevertheless, severe corrosion and deterioration of the coatings was not detected for all the inhibitor-enriched coatings. This proves that the composite coating system has released corrosion inhibitors to suppress the corrosion propagation and provide active corrosion protection to Mg alloy.

In order to evaluate the self-healing capability as well as to obtain the corrosion kinetics of the four samples, the peak anodic and cathodic current density at each read-point for all specimens are summarized in Fig. 8. Note, Fig 8 contains the results of additional measurement (compared to Fig. 7), recorded at 24 hours. For coatings without inhibitor, a sharp increase of corrosion activity was observed after 36 hours of immersion in NaCl solution. After 48 h the sum of positive and negative peak current density rose to above 400

μA cm^{-2}, indicating the occurrence of severe corrosion. As for coating impregnated with inhibitors, the corresponding values of peak current density remains 5 to 100 times lower at all measured immersion durations demonstrating effective mitigation of corrosion process.

Fig. 9 and 10 demonstrate the SEM/EDS analysis of the defect after SVET measurement for AZ_PEO_SG and AZ_PEO_Gly_SG sample. It can be seen that the surrounding areas of the artificial defect on the reference coating were covered with needle-like corrosion products, which are likely to be $Mg(OH)_2$. However, the inner and peripheral regions of the defect were relatively smooth and free of large volume of corrosion products for the inhibitor-containing coating. EDS results (Fig. 10) were based on the corresponding areas of the sol-gel layer indicated by two red rectangles in Fig. 9(e) and (f). The EDS analysis of the AZ_PEO_SG with needle-like products revealed the presence of higher amount of magnesium than that of AZ_PEO_Gly_SG. This further proves the existence of $Mg(OH)_2$ on the adjacent regions of the defect.

Fig. 11 illustrates the corrosion and inhibition mechanism for coating with and without the inhibitors. For the reference coating, once the corrosive ions penetrate to the substrate, highly active Mg rapidly corroded and formed $Mg(OH)_2$. This is well corroborated by precipitation of numerous needle-like corrosion products observed on the edge of the artificial defect in Fig. 10(a). For the coating enriched with inhibitors, two mechanisms can account for the superior anti-corrosion capability: (1) some organic functional groups in the inhibitors (like carboxyl, hydroxyl, etc.) can adsorb on the Mg surface and decrease the effective anodic area, therefore decelerating Mg dissolution; (2) inhibitors can form stable chelate complexes with detrimental impurities in Mg alloys, eliminating their opportunity to re-deposit on Mg surface. Since harmful impurities, like iron, can enlarge cathodically active sites on Mg surface by re-deposition, inhibitors released from the hybrid coating can drastically prevent Fe re-deposition and therefore strongly inhibit the corrosion process of Mg [50-56]. Therefore, the active protection mechanism of the coating was achieved by suppression of the re-deposition of detrimental impurity and/or adsorption upon the exposed surface from incorporated inhibitor.

4. Conclusions

1) Three organic Mg corrosion inhibitors, sodium salts of glycolic, 4-aminosalicylic and 2,6-pyridinedicarboxylic acids, have been successfully incorporated and immobilized into the porous PEO coating by sealing with a top sol-gel layer.

2) Compared with the blank coating, all inhibitor-containing composite coatings demonstrated superior corrosion resistance and provide active corrosion protection for Mg alloy AZ91.

3) The release of the inhibitors results in active corrosion protection and self-healing property for PEO coated Mg.

Acknowledgement

The technical support of Mr. Volker Heitmann and Mr. Ulrich Burmester during this work is gratefully acknowledged. Dr. S.V. Lamaka acknowledges the financial support of Alexander von Humboldt Foundation via Experienced Researcher Grant. The authors would like to acknowledge the financial support of the Shanghai Pujiang Program (NO. 19PJ1431500), National Natural Science Foundation of China (NO. U1737102, 51531007, 51771050 and 51771122), Young Elite Scientists Sponsorship Program by CAST (2017QNRC001), National Program for Young Top-notch Professionals and the Fundamental Research Funds for the Central Universities (N170203006 and N170205002).

References

[1] T.S.N.S. Narayanan, Il Song Park, M.H. Lee, Strategies to improve the corrosion resistance of microarc oxidation (MAO) coated magnesium alloys for degradable implants: Prospects and challenges, Progress in Materials Science. 60 (2014) 1–71.

[2] L. Zhang, J. Zhang, C.-F. Chen, Y. Gu, Advances in microarc oxidation coated AZ31 Mg alloys for biomedical applications, Corrosion Science. 91 (2015) 7–28.

[3] X. Lu, M. Mohedano, C. Blawert, E. Matykina, R. Arrabal, K.U. Kainer, Plasma electrolytic oxidation coatings with particle additions – A review, Surface and Coatings Technology. 307 (2016) 1165–1182.

[4] K. Nielsch, J. Choi, K. Schwirn, R.B. Wehrspohn, U. Gösele, Self-ordering Regimes of Porous Alumina: The 10 Porosity Rule, Nano Lett. 2 (2002) 677–680.

[5] M. Esmaily, J.E. Svensson, S. Fajardo, N. Birbilis, G.S. Frankel, S. Virtanen, R. Arrabal, S. Thomas, L.G. Johansson, Fundamentals and advances in magnesium alloy corrosion, Progress in Materials Science. 89 (2017) 92-193.

[6] Gh. Barati Darband, M. Aliofkhazraei, P. Hamghalam, N. Valizade, Plasma electrolytic oxidation of magnesium and its alloys: Mechanism, properties and applications, Journal of Magnesium and Alloys. 5 (2017) 74-132.

[7] X. Lu, C. Blawert, M.L. Zheludkevich, K.U. Kainer, Insights into plasma electrolytic oxidation treatment with particle addition, Corrosion Science. 101 (2015) 201–207.

[8] X. Lu, C. Blawert, D. Tolnai, T. Subroto, K.U. Kainer, T. Zhang, F. Wang, M.L. Zheludkevich, 3D reconstruction of plasma electrolytic oxidation coatings on Mg alloy via synchrotron radiation tomography, Corrosion Science, 139 (2018) 395-402.
[9] X. Lu, C. Blawert, K.U. Kainer, T. Zhang, F. Wang, M.L. Zheludkevich, Influence of particle additions on corrosion and wear resistance of plasma electrolytic oxidation coatings on Mg alloy, Surface and Coatings Technology, 352 (2018) 1-14.
[10] R. Arrabal, E. Matykina, F. Viejo, P. Skeldon, G.E. Thompson, Corrosion resistance of WE43 and AZ91D magnesium alloys with phosphate PEO coatings, Corrosion Science. 50 (2008) 1744–1752.
[11] R.O. Hussein, D.O. Northwood, X. Nie, The effect of processing parameters and substrate composition on the corrosion resistance of plasma electrolytic oxidation (PEO) coated magnesium alloys, Surface and Coatings Technology. 237 (2013) 357–368.
[12] Y. Chen, X. Lu, C. Blawert, M.L. Zheludkevich, T. Zhang, F. Wang, Formation of self-lubricating PEO coating via in-situ incorporation of PTFE particles, Surface and Coatings Technology. 337 (2018) 379–388.
[13] Y. Song, K. Dong, D. Shan, E.-H. Han, Study of the formation process of titanium oxides containing micro arc oxidation film on Mg alloys, Applied Surface Science. 314 (2014) 888–895.
[14] Y. Song, K. Dong, D. Shan, E.-H. Han, Investigation of a novel self-sealing pore micro-arc oxidation film on AM60 magnesium alloy, Journal of Magnesium and Alloys. 1 (2013) 82–87.
[15] S. Stojadinović, R. Vasilić, J. Radić-Perić, M. Perić, Characterization of plasma electrolytic oxidation of magnesium alloy AZ31 in alkaline solution containing fluoride, Surface and Coatings Technology. 273(2015) 1–11.
[16] Y. Mori, A. Koshi, J. Liao, H. Asoh, S. Ono, Characteristics and corrosion resistance of plasma electrolytic oxidation coatings on AZ31B Mg alloy formed in phosphate – Silicate mixture electrolytes, Corrosion Science. 88 (2014) 254–262.
[17] T.W. Clyne, S.C. Troughton, A review of recent work on discharge characteristics during plasma electrolytic oxidation of various metals, International Materials Reviews. 64 (2018) 127–162.
[18] R.-C. Zeng, L.-Y. Cui, K. Jiang, R. Liu, B.-D. Zhao, Y.-F. Zheng, In Vitro Corrosion and Cytocompatibility of a Microarc Oxidation Coating and Poly(L-lactic acid) Composite Coating on Mg-1Li-1Ca Alloy for Orthopedic Implants, ACS Appl Mater Interfaces. 8 (2016) 10014–10028.
[19] L. Yu, J. Cao, Y. Cheng, An improvement of the wear and corrosion resistances of AZ31 magnesium alloy by plasma electrolytic oxidation in a silicate–hexametaphosphate electrolyte with the suspension of SiC nanoparticles, Surface and Coatings Technology. 276 (2015) 266–278.
[20] B.-S. Lou, Y.-Y. Lin, C.-M. Tseng, Y.-C. Lu, J.-G. Duh, J.-W. Lee, Plasma electrolytic oxidation coatings on AZ31 magnesium alloys with Si3N4 nanoparticle additives, Surface and Coatings Technology. 332 (2017) 358–367.
[21] W.A. Zoubi, M.P. Kamil, Y.G. Ko, Synergistic influence of inorganic oxides (ZrO_2 and SiO_2) with N_2H_4 to protect composite coatings obtained via plasma electrolyte oxidation on Mg alloy, Physical Chemistry Chemical Physics. 19 (2017) 2372–2382.
[22] M. Mohedano, R. Arrabal, B. Mingo, A. Pardo, E. Matykina, Role of particle type and concentration on characteristics of PEO coatings on AM50 magnesium alloy, Surface and Coatings Technology. 334 (2018) 328–335.
[23] M. Mohedano, C. Blawert, M.L. Zheludkevich, Cerium-based sealing of PEO coated AM50 magnesium alloy, Surface and Coatings Technology. 269 (2015) 145–154.
[24] U. Malayoglu, K.C. Tekin, S. Shrestha, Influence of post-treatment on the corrosion resistance of PEO coated AM50B and AM60B Mg alloys, Surface and Coatings Technology. 205 (2010) 1793–1798.
[25] X. Lin, L. Tan, P. Wan, X. Yu, K. Yang, Z. Hu, et al., Characterization of micro-arc oxidation coating post-treated by hydrofluoric acid on biodegradable ZK60 magnesium alloy, Surface and Coatings Technology. 232 (2013) 899–905.

[26] B. Mingo, R. Arrabal, M. Mohedano, Y. Llamazares, E. Matykina, A. Yerokhin, et al., Influence of sealing post-treatments on the corrosion resistance of PEO coated AZ91 magnesium alloy, Applied Surface Science. 433 (2018) 653–667.
[27] D.K. Ivanou, M. Starykevich, A.D. Lisenkov, M.L. Zheludkevich, H.B. Xue, S.V. Lamaka, M.G.S. Ferreira. Plasma anodized ZE41 magnesium alloy sealed with hybrid epoxy-silane coating, Corrosion Science. 73 (2013) 300–308.
[28] S.V. Gnedenkov, S.L. Sinebryukhov, D.V. Mashtalyar, K.V. Nadaraia, D.P. Kiryukhin, G.A. Kichigina, P.P. Kushch, V.M. Buznik, Composite coatings formed on the PEO-layers with the use of solutions of tetrafluoroethylene telomers, Surface and Coatings Technology. 346 (2018) 53-62.
[29] S.V. Lamaka, G. Knörnschild, D.V. Snihirova, M.G. Taryba, M.L. Zheludkevich, M.G.S. Ferreira, Complex anticorrosion coating for ZK30 magnesium alloy, Electrochimica Acta. 55 (2009) 131–141.
[30] D.K. Ivanou, K.A. Yasakau, S. Kallip, A.D. Lisenkov, M. Starykevich, S.V. Lamaka, et al. Active corrosion protection coating for a ZE41 magnesium alloy created by combining PEO and sol–gel techniques, RSC Adv. 6 (2016) 12553–12560.
[31] A. Mesbah, C. Juers, F. Lacouture, S. Mathieu, E. Rocca, M. François, et al. Inhibitors for magnesium corrosion: Metal organic frameworks, Solid State Sciences. 9 (2007) 322–328.
[32] X. Yang, F.S. Pan, D.F. Zhang, A Study on Corrosion Inhibitor for Magnesium Alloy, Materials Science Forum. 610-613 (2009) 920–926.
[33] A.F. Galio, S.V. Lamaka, M.L. Zheludkevich, L.F.P. Dick, I.L. Müller, M.G.S. Ferreira, Inhibitor-doped sol–gel coatings for corrosion protection of magnesium alloy AZ31, Surface and Coatings Technology. 204 (2010) 1479–1486.
[34] T.N. Ostanina, V.M. Rudoi, A.N. Ovsyannikova, V.B. Malkov, Magnesium alloys spontaneous dissolution features under external anodic polarization in presence of inhibitors, Russian Journal of Electrochemistry. 46 (2010) 707–713.
[35] X.P. Guo, G.L. Song, J.Y. HU, D.B. HUANG, Corrosion inhibition of magnesium (Mg) Alloys, in: Corrosion Prevention of Magnesium Alloys, Woodhead Publishing Limited, 2013: pp. 61–84.
[36] J. Hu, D. Zeng, Z. Zhang, T. Shi, G.-L. Song, X. Guo, 2-Hydroxy-4-methoxy-acetophenone as an environment-friendly corrosion inhibitor for AZ91D magnesium alloy, Corrosion Science. 74 (2013) 35–43.
[37] N. Dinodi, A.N. Shetty, Alkyl carboxylates as efficient and green inhibitors of magnesium alloy ZE41 corrosion in aqueous salt solution, Corrosion Science. 85 (2014) 411–427.
[38] N. Dang, Y.H. Wei, L.F. Hou, Y.G. Li, C.L. Guo, Investigation of the inhibition effect of the environmentally friendly inhibitor sodium alginate on magnesium alloy in sodium chloride solution, Materials and Corrosion. 66 (2015) 1354–1362.
[39] I.A. Kartsonakis, S.G. Stanciu, A.A. Matei, E.K. Karaxi, R. Hristu, A. Karantonis, et al., Evaluation of the protective ability of typical corrosion inhibitors for magnesium alloys towards the Mg ZK30 variant, Corrosion Science. 100 (2015) 194–208.
[40] J. Sullivan, N. Cooze, C. Gallagher, T. Lewis, T. Prosek, D. Thierry, In situ monitoring of corrosion mechanisms and phosphate inhibitor surface deposition during corrosion of zinc-magnesium-aluminium (ZMA) alloys using novel time-lapse microscopy, Faraday Discussions. 180 (2015) 361–379.
[41] P. Zhang, Q. Li, L.Q. Li, X.X. Zhang, Z.W. Wang, A study of environment-friendly synergistic inhibitors for AZ91D magnesium alloy, Materials and Corrosion. 66 (2013) 31–34.
[42] M.A. Deyab, Decyl glucoside as a corrosion inhibitor for magnesium-air battery, Journal of Power Sources. 325 (2016) 98–103.
[43] Y. Li, Z.X. Ba, Y.L. Li, Y. Ge, X.C. Zhu, Influence of sodium alginate inhibitor addition on the corrosion protection performance of AZ91D magnesium alloy in NaCl solution, Anti-Corrosion Meth & Material. 64 (2017) 486–491.

[44] V. Upadhyay, Z. Bergseth, B. Kelly, D. Battocchi, Silica-Based Sol-Gel Coating on Magnesium Alloy with Green Inhibitors, Coatings. 7 (2017) 1–11.
[45] G. Williams, H.N. McMurray, R. Grace, Inhibition of magnesium localised corrosion in chloride containing electrolyte, Electrochimica Acta. 55 (2010) 7824–7833.
[46] X. Lu, Y. Li, P. Ju, Y. Chen, J. Yang, K. Qian, T. Zhang, F. Wang, Unveiling the inhibition mechanism of an effective inhibitor for AZ91 Mg alloy, Corrosion Science. 148 (2019) 264-271.
[47] M. Sun, A. Yerokhin, M.Y. Bychkova, D.V. Shtansky, E.A. Levashov, A. Matthews, Self-healing plasma electrolytic oxidation coatings doped with benzotriazole loaded halloysite nanotubes on AM50 magnesium alloy, Corrosion Science. 111 (2016) 753–769.
[48] A.S. Gnedenkov, S.L. Sinebryukhov, D.V. Mashtalyar, S.V. Gnedenkov, Protective properties of inhibitor-containing composite coatings on a Mg alloy, Corrosion Science. 102 (2016) 348–354.
[49] A.S. Gnedenkov, S.L. Sinebryukhov, D.V. Mashtalyar, S.V. Gnedenkov, Localized corrosion of the Mg alloys with inhibitor-containing coatings: SVET and SIET studies, Corrosion Science. 102 (2016) 269–278.
[50] J. Yang, C. Blawert, S.V. Lamaka, D. Snihirova, X. Lu, S. Di, et al., Corrosion protection properties of inhibitor containing hybrid PEO-epoxy coating on magnesium, Corrosion Science. 140 (2018) 99–110.
[51] S.V. Lamaka, B. Vaghefinazari, D. Mei, R.P. Petrauskas, D. Höche, M.L. Zheludkevich, Comprehensive screening of Mg corrosion inhibitors, Corrosion Science. 128 (2017) 224–240.
[52] E. L. Silva, S. V. Lamaka, Di Mei, M.L. Zheludkevich, The Reduction of Dissolved Oxygen During Magnesium Corrosion, Chemistry Open. 7 (2018) 664-68.
[53] D. Hoche, C. Blawert, S.V. Lamaka, N. Scharnagl, C. Mendis, M.L. Zheludkevich, The effect of iron re-deposition on the corrosion of impurity-containing magnesium, Physical chemistry chemical physics : PCCP. 18 (2016) 1279-1291.
[54] J. Li, W. Sun, B. Hurley, A.A. Luo, R.G. Buchheit, Cu redistribution study during the corrosion of AZ91 using a rotating ring-disk collection experiment, Corrosion Science. 112 (2016) 760-764.
[55] D. Mercier, J. Światowska, S. Zanna, A. Seyeux, P. Marcus, Role of Segregated Iron at Grain Boundaries on Mg Corrosion, Journal of The Electrochemical Society. 165 (2018) C42-C49.
[56] E. Michailidou, H.N. McMurray, G. Williams, Quantifying the Role of Transition Metal Electrodeposition in the Cathodic Activation of Corroding Magnesium, Journal of The Electrochemical Society. 165 (2018) C195-C205.

Figure captions

Fig. 1 The surface morphology of PEO coating on AZ91D Mg alloy (a) overview of uniformly distributed pores; (b) at higher magnification; (c) sealed with the sol-gel coating, AZ_PEO_SG.

Fig. 2 SEM micrograph and EDS mapping analysis of the cross-section of the AZ_PEO_SG coating.

Fig. 3 Hydrogen evolution curves for AZ91 Mg in 0.5% NaCl with or without inhibitors.

Fig. 4 Evolution of Bode spectra for four PEO-SG composite coatings in 0.5wt% NaCl solution: (a) AZ_PEO_SG; (b) AZ_PEO_Gly_SG; (c) AZ_PEO_4AmSal_SG; (d) AZ_PEO_PDC_SG.

Fig. 5 Electric equivalent circuits used for impedance fitting for PEO-SG composite coatings at different stages of corrosion.

Fig. 6 Evolution of parameters depicted in Fig. 4 during immersion in 0.5wt% NaCl electrolyte: (a) sol-gel coating resistance; (b) mixed PEO-SG layer resistance; (c) dense layer resistance (polarization resistance for AZ_PEO_SG sample after 2 h).

Fig. 7 Optical images of the PEO-SG samples and SVET maps of current recorded above the surface of the PEO-SG samples. The time of exposure and inhibitors are indicated.

Fig. 8 Evolution of peak anodic and cathodic current density for four PEO-SG samples.

Fig. 9 SEM images of the artificial defects in PEO-SG coatings after immersion and SVET studies. (a) (c) (e) AZ_PEO_SG sample; (b) (d) (f) AZ_PEO_Gly_SG sample.

Fig. 10 EDS results of the PEO-SG coatings after immersion and SVET studies: (a)AZ_PEO_SG sample; (b) AZ_PEO_Gly_SG sample. Taken at the locations marked as red rectangles in Fig. 9.

Fig. 11 Schematic diagram for corrosion & inhibition mechanism for composite coatings (a) without and (b) with inhibitors.

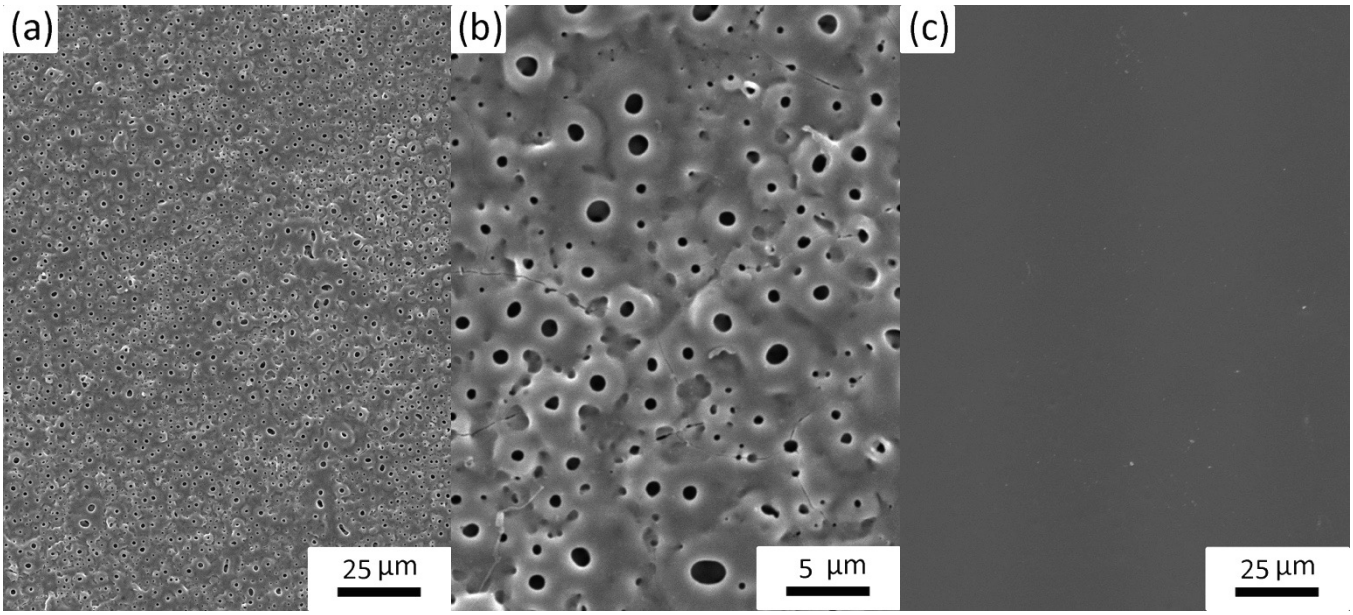

Fig. 1 The surface morphology of PEO coating on AZ91D Mg alloy (a) overview of uniformly distributed pores; (b) at higher magnification; (c) sealed with the sol-gel coating, AZ_PEO_SG.

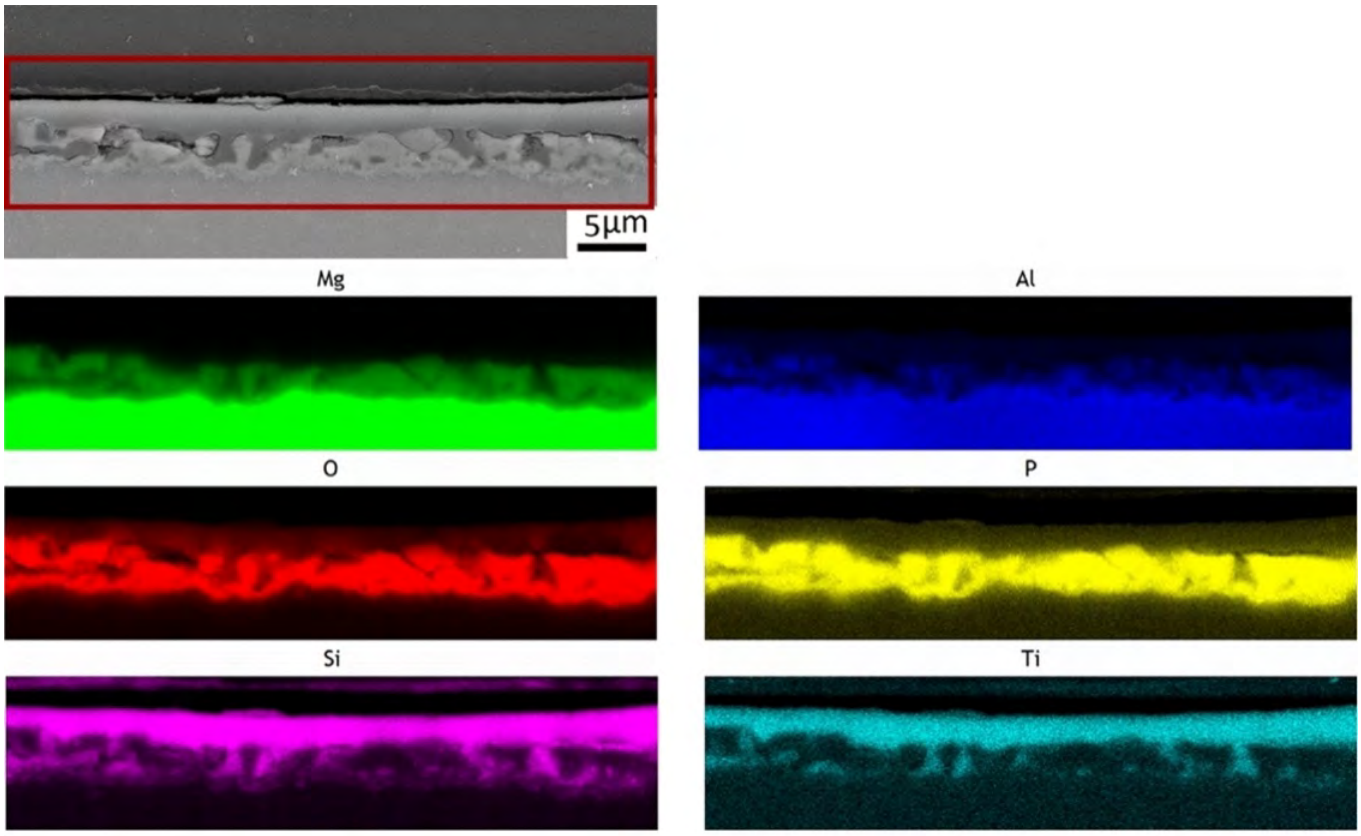

Fig. 2 SEM micrograph and EDS mapping analysis of the cross-section of the AZ_PEO_SG coating.

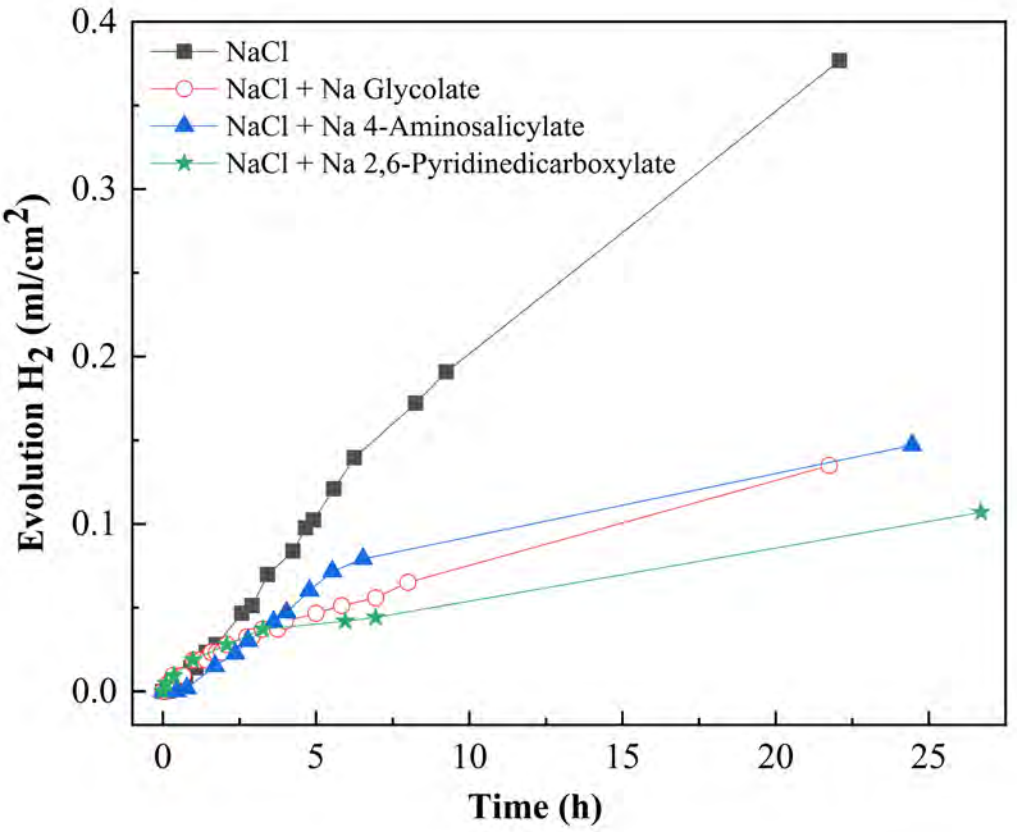

Fig. 3 Hydrogen evolution curves for AZ91 Mg in 0.5% NaCl with or without inhibitors.

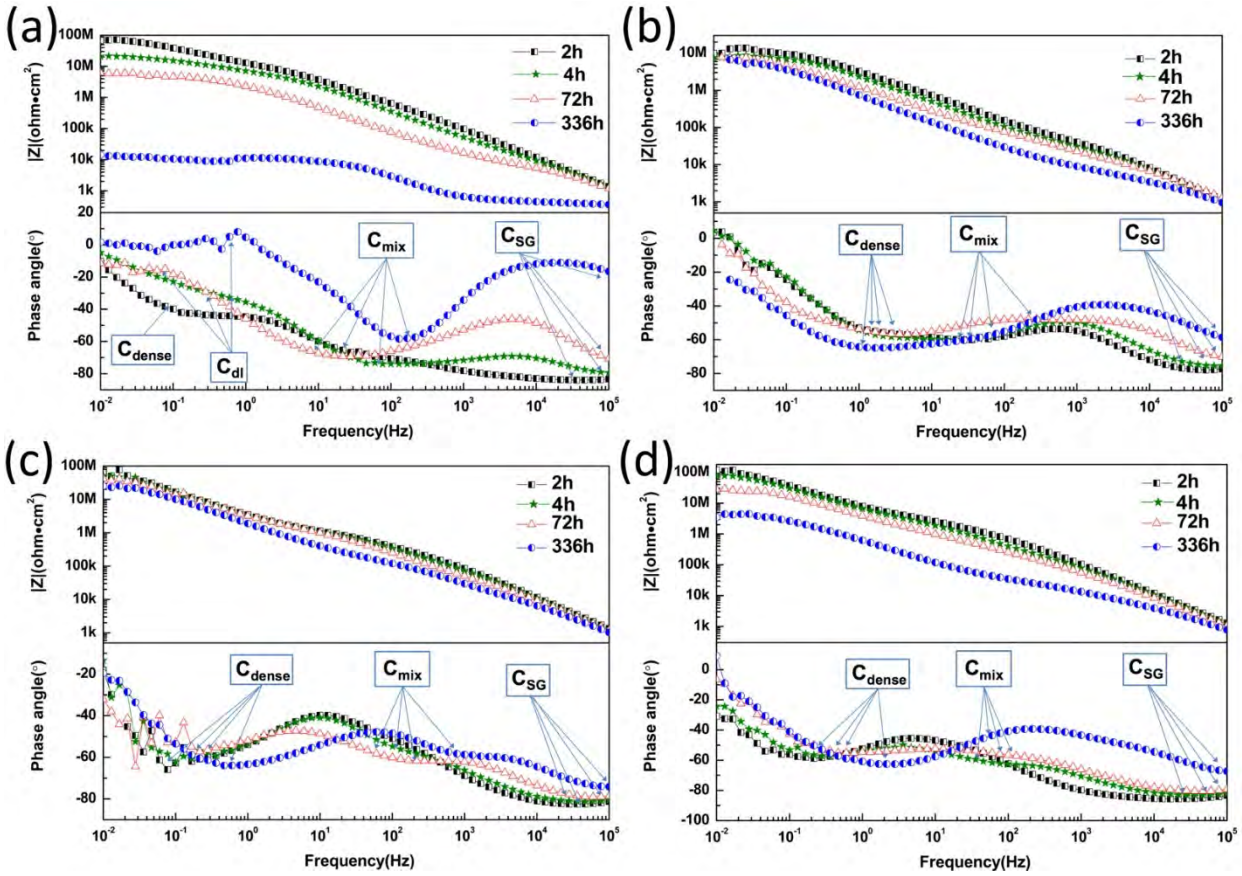

Fig. 4 Evolution of Bode spectra for four PEO-SG composite coatings in 0.5wt% NaCl solution: (a) AZ_PEO_SG; (b) AZ_PEO_Gly_SG; (c) AZ_PEO_4AmSal_SG; (d) AZ_PEO_PDC_SG.

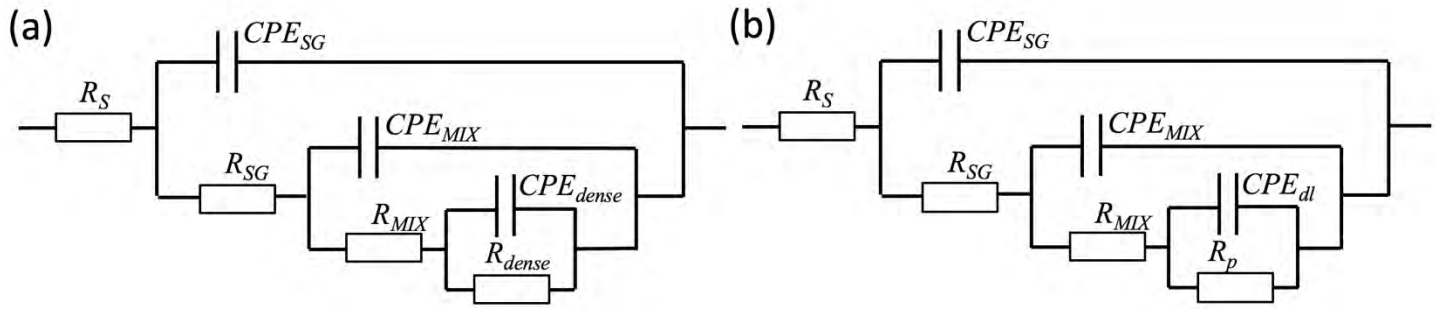

Fig. 5 Electric equivalent circuits used for impedance fitting for PEO-SG composite coatings at different stages of corrosion.

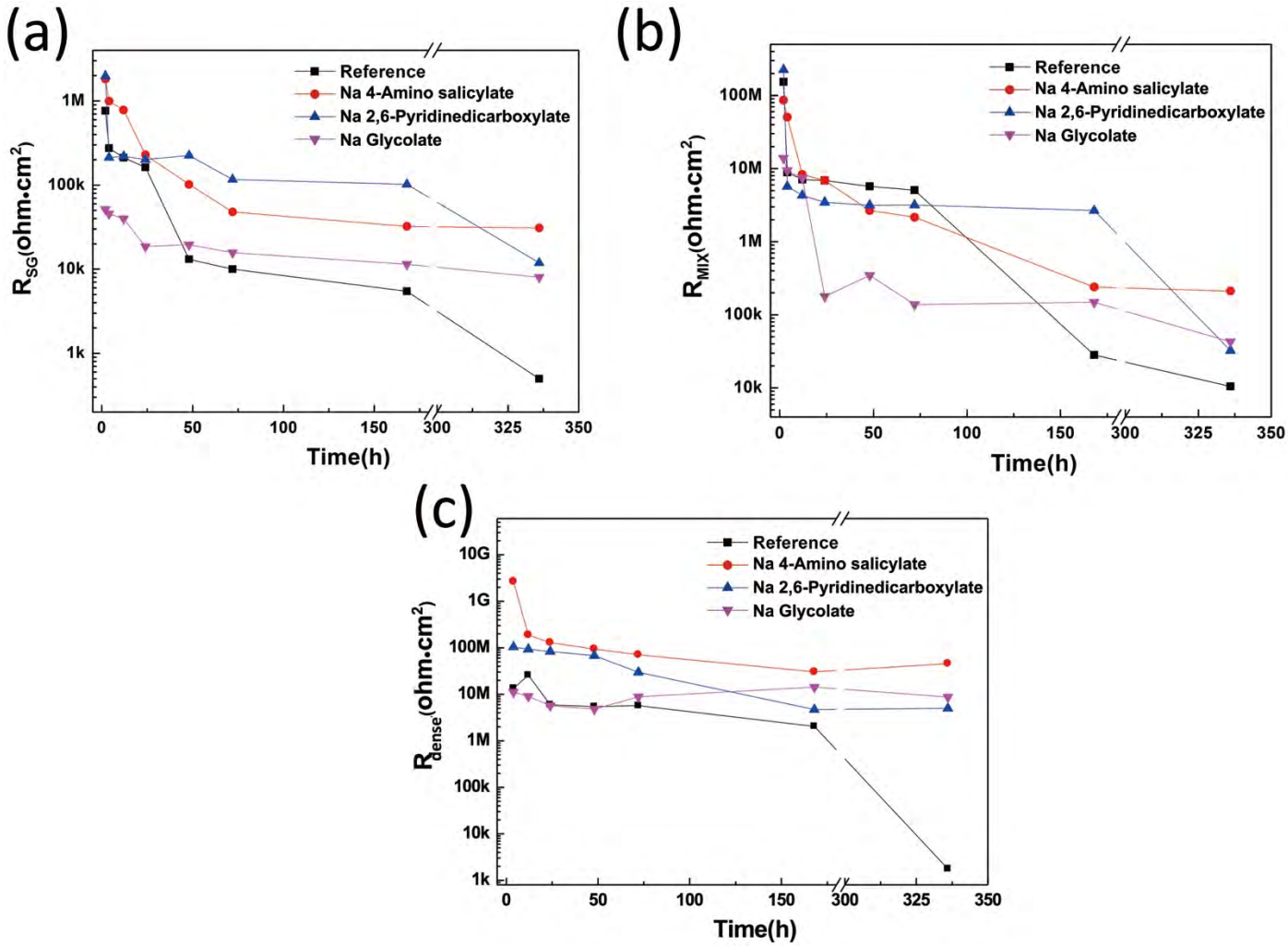

Fig. 6 Evolution of parameters depicted in Fig. 4 during immersion in 0.5wt% NaCl electrolyte: (a) sol-gel coating resistance; (b) mixed PEO-SG layer resistance; (c) dense layer resistance (polarization resistance for AZ_PEO_SG sample after 2 h).

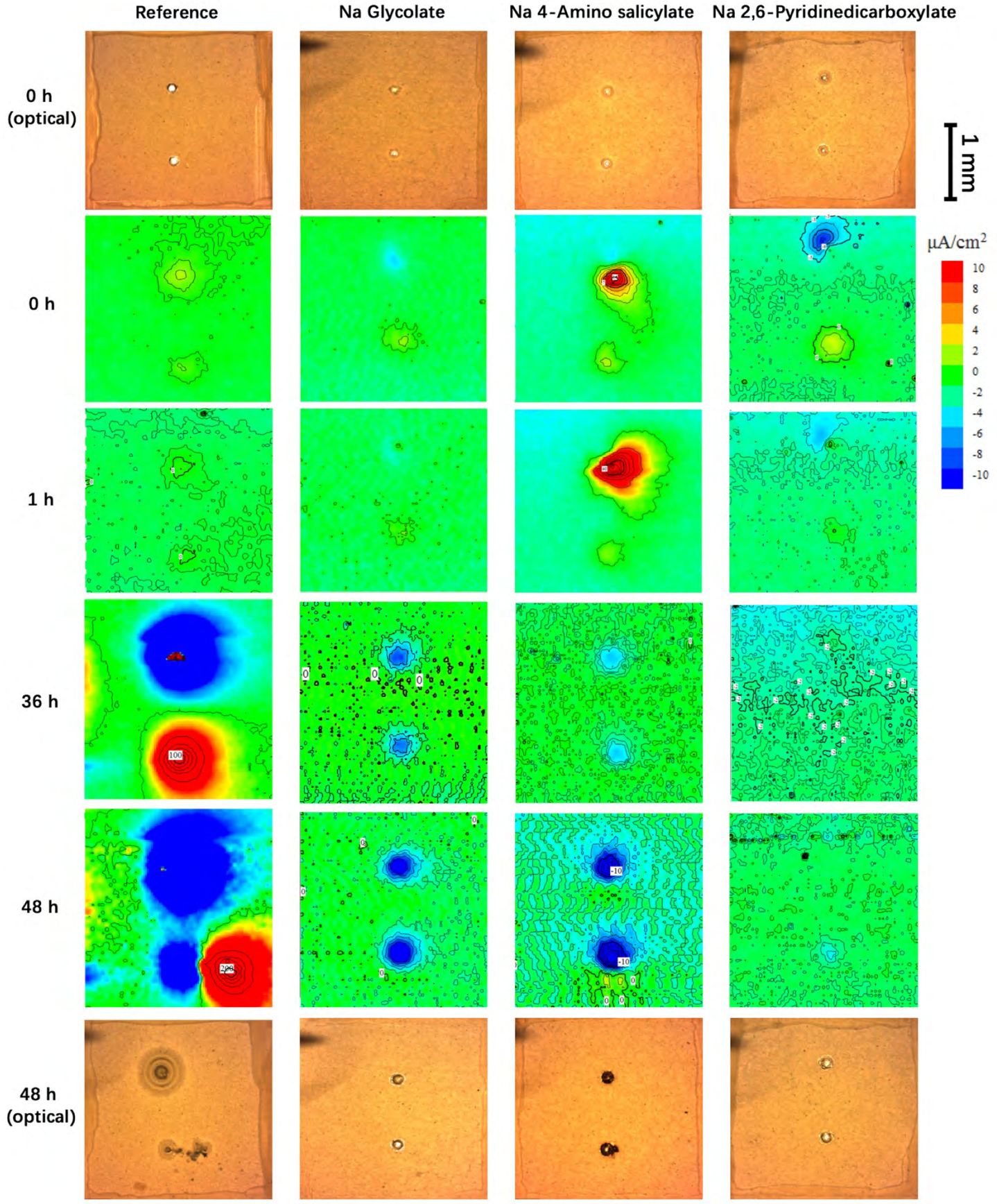

Fig. 7 Optical images of the PEO-SG samples and SVET maps of current recorded above the surface of the PEO-SG samples. The time of exposure and inhibitors are indicated.

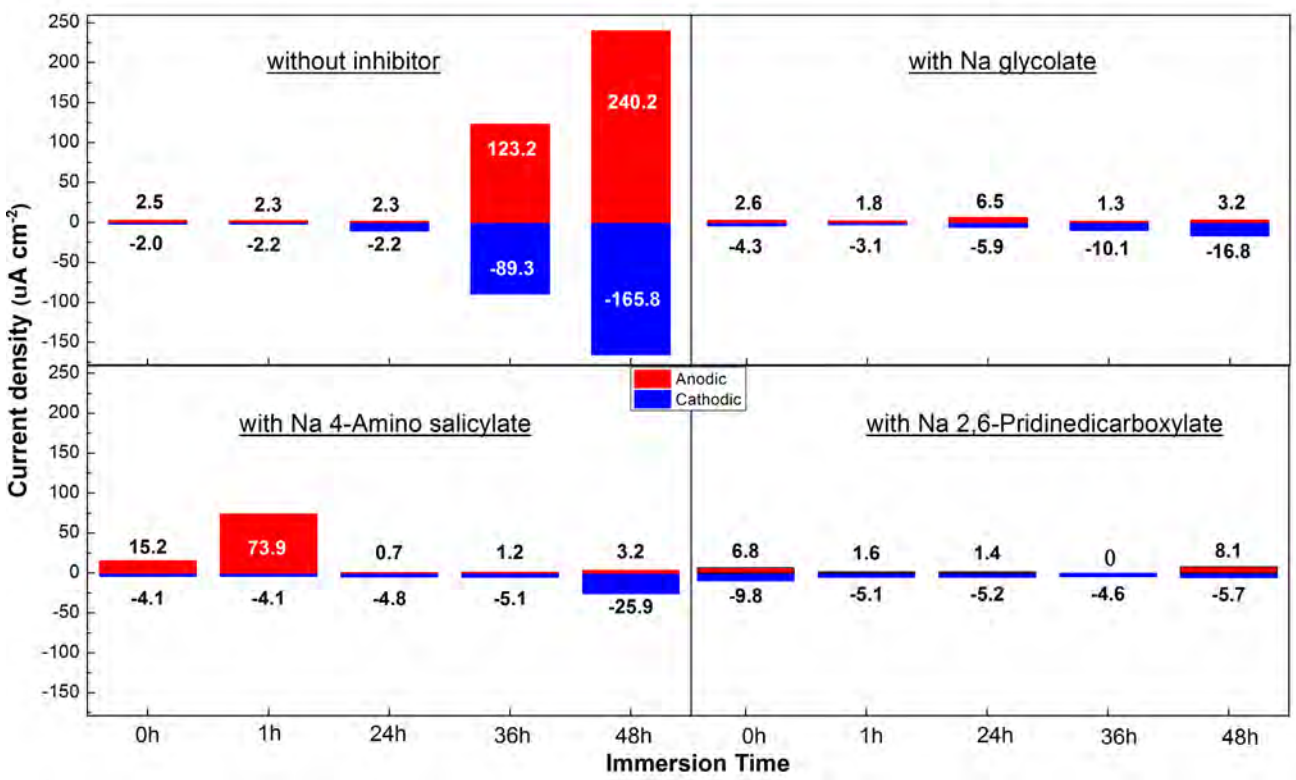

Fig. 8 Evolution of peak anodic and cathodic current density for four PEO-SG samples.

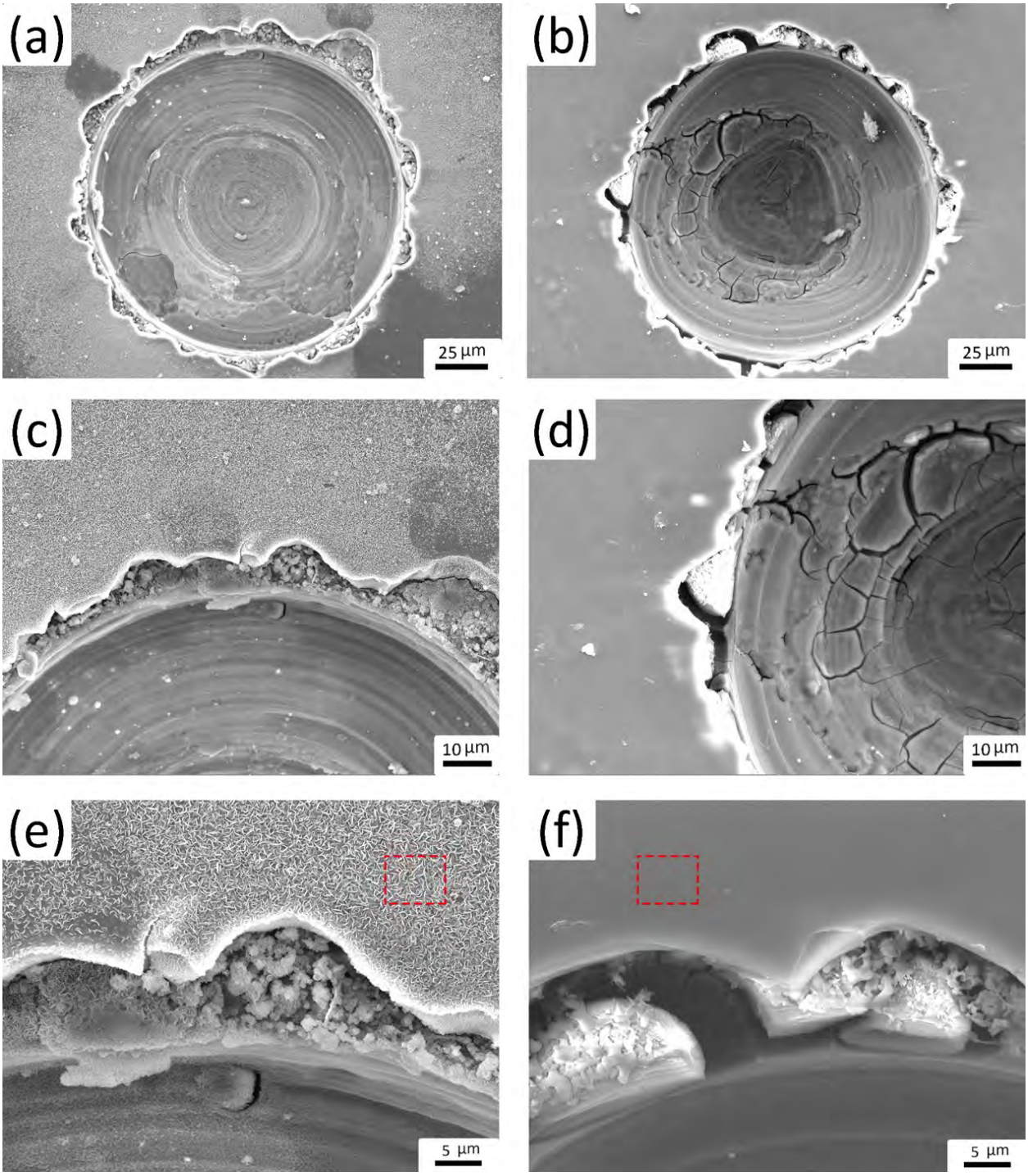

Fig. 9 SEM images of the artificial defects in PEO-SG coatings after immersion and SVET studies. (a) (c) (e) AZ_PEO_SG sample; (b) (d) (f) AZ_PEO_Gly_SG sample.

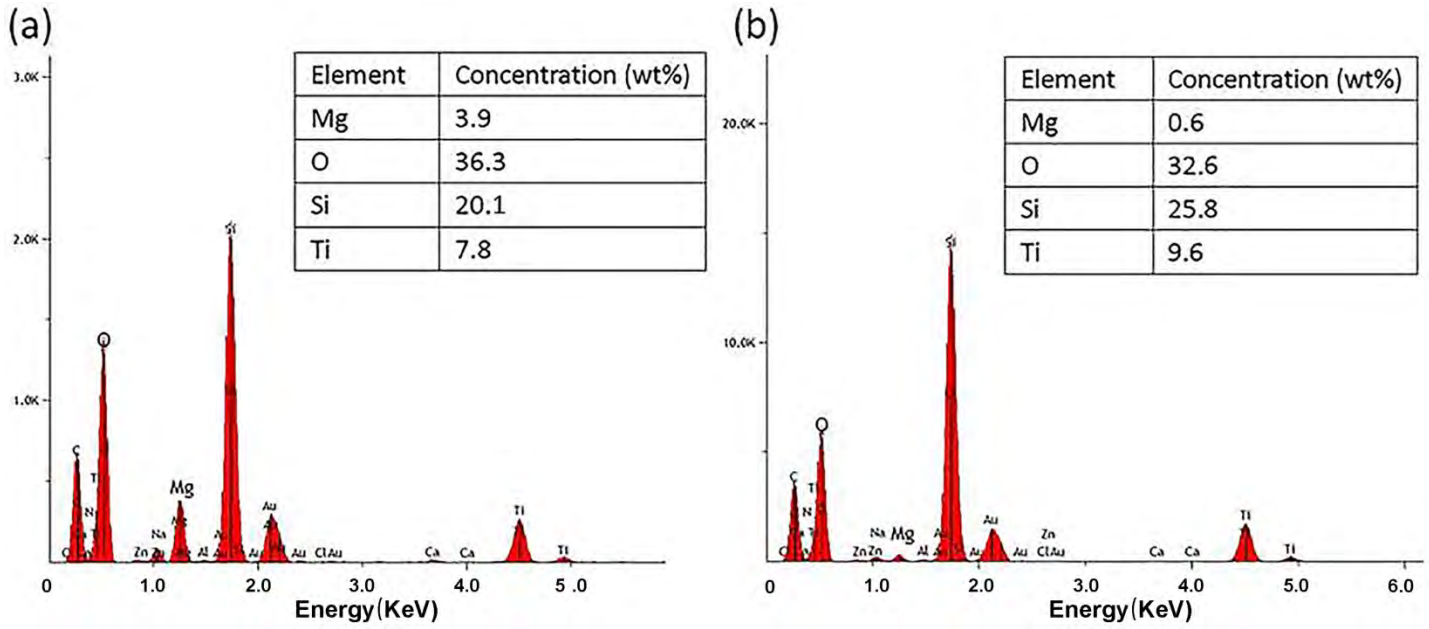

Fig. 10 EDS results of the PEO-SG coatings after immersion and SVET studies: (a)AZ_PEO_SG sample; (b) AZ_PEO_Gly_SG sample. Taken at the locations marked as red rectangles in Fig. 9.

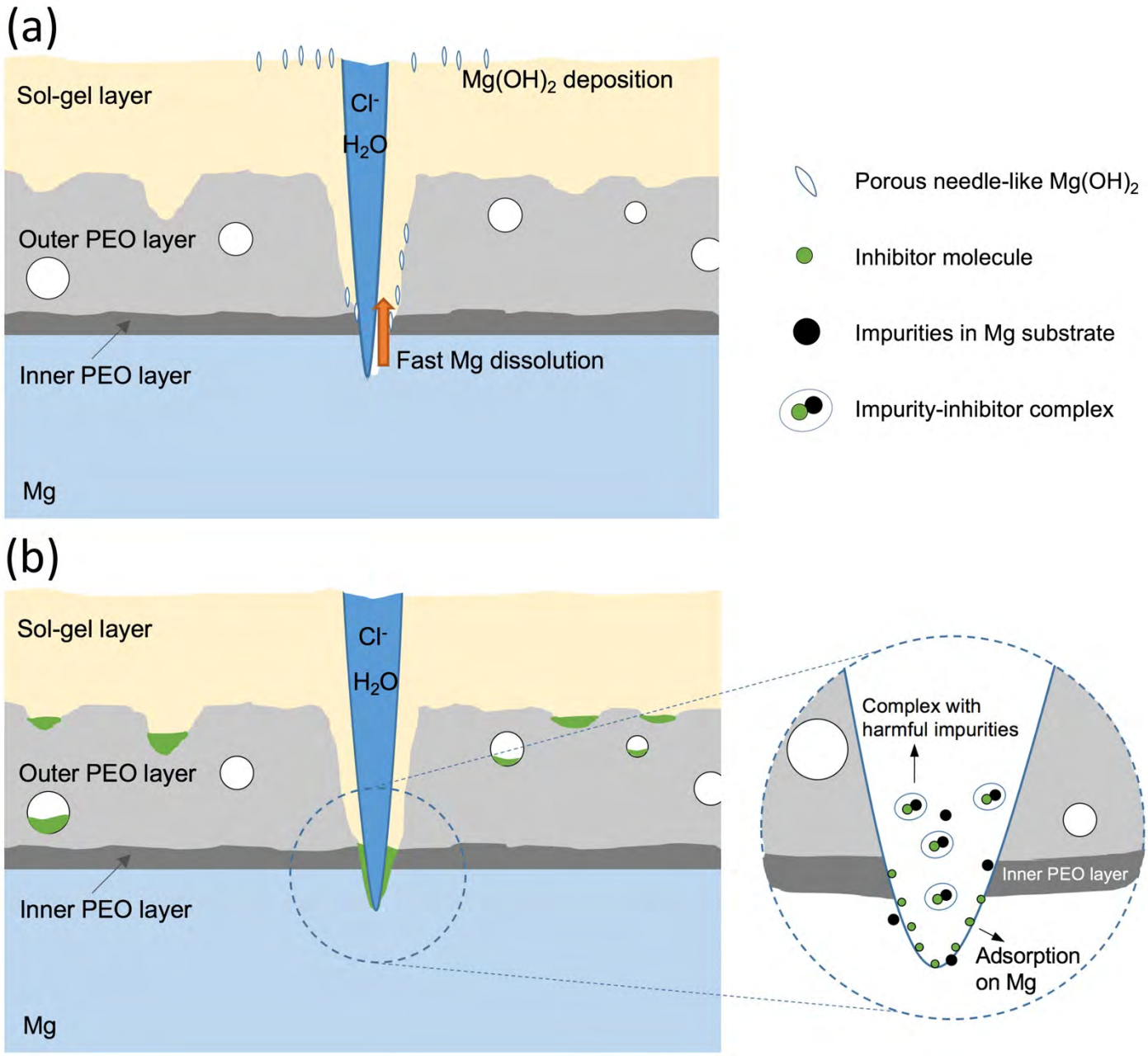

Fig. 11 Schematic diagram for corrosion & inhibition mechanism for composite coatings (a) without and (b) with inhibitors.